International Journal of Scientific Research and Engineering Development-– Volume 5 Issue 3, May-June 2022

Available at www.ijsred.com

RESEARCH ARTICLE OPEN ACCESS

Design and simulation of a 500kVA power Electronic Transformer for Distribution Network

Ereola Aladesanmi *, Priye Kenneth Ainah**

*Department of Electrical, Electronic and Computer Engineering,
University of KwaZulu-Natal, Durban, South Africa
ereolaa@yahoo.com.

** Department Electrical and Electronic Engineering, Niger Delta University,
Amassoma, Wilberforce Island, Bayelsa State, Nigeria
ainahpriye@ndu.edu.ng

----------**********----------

Abstract:

The paper presents the design, modeling and simulation of a three-stage power electronic transformer (PET), for use in the low voltage (LV) distribution network. The PET device consists of three stages (input stage, isolation stage and output stage), and the parameters of the stages were calculated based on a 11/0.415 kV LV distribution network specifications. The device uses converters (AC-DC-AC-DC-AC), and a high frequency transformer (HFT) to supply the desired voltage and power to the load. The PET device is modeled and simulated on the MATLAB/SIMULINK software. The simulation results show a perfect voltage and current waveform and the ability of the PET device to adjust to different load conditions.

The device performs very well (meet the design specifications of 11/0.415kV for LV distribution network) and can displace the traditional transformers in the future smart grid.

Keywords **—Power electronic transformer, high-frequency transformer, Simulink, distribution network**

----------**********----------

I. INTRODUCTION

Electrical power transformers are static components in power system networks that are responsible for voltage conversion. Traditional line frequency transformers (LFTs) are reliable, inexpensive, efficient, and simple to construct [1], [2]. However, they have bulky size, heavy weight, poor voltage, and current regulation during grid disturbances, environmental unfriendly due to the use of mineral oil, and heavy inrush currents due to core saturation [3].

With the recent technological evolutions, power electronic transformer is seen as one of the emerging technologies to overcome these drawbacks and enhance future smart grids [4], [5]. Aside from overcoming the aforementioned drawbacks of the traditional line frequency, power electronic transformer poses some advantages over LFT such as voltage control, reverse power flow control, galvanic isolation, Reactive power reparation, bi-directional power flow, fault current detection, protection, harmonic block, and voltage sag compensation are some of the advantages [6]–[9]. Power electronic transformers can be used as an interface between generation sources and distribution networks, between two distribution networks, and between distribution networks and loads. Also, PET can supply loads with the required voltage and frequency levels without an additional power transformer and frequency conversion devices. It can also effectively control fault current

without additional protection relays [1]. Nevertheless, PET has some drawback which includes; the high cost of implementation, complexity in design, and the efficiency iis hard to compare to LFT [10], [11].

The principle of operation and the dynamic simulation of the steady-state characteristic of the PET is presented in this paper.

II. POWER ELECTRONIC TRANSFORMER CONFIGURATIONS AND APPLICATION

PET is a 3-stage power conversion device that converts medium voltage (MV) to LV and enhances direct current (DC) grid connections [9]. PET enhances load identification and control, reverse power flow mitigation, and render solutions to power quality issues such as voltage swell and sag on the grid [12], [13]. The technology was developed in 1970 but the application of the model was restricted due to the LV, availability of circuit topologies and rating of the power switches. Due to the recent development in technology, different topologies of PETs such as smart transformers, solid-state transformers, intelligent universal transformers, etc, have emerged. There are three basic configurations of PET such as single-stage, two-stage, and 3-stage [6], [9], [14] as shown in Fig 1.

A. Single-stage configuration

The medium AC voltage is converted directly to low AC voltage in the Single-stage via a HFT without the DC link capacitor. The stage has high efficiency and reliability when compared to other stages because it does not have switching losses and conductor. The direction of the power flow and magnitude are controlled by phase shift angle as given in Eq.1 [15], [16].

$$P_O = \frac{V_i V_O}{X_p}\left(\varphi - \frac{\varphi^2}{\pi}\right) \qquad (1)$$

where, X_p is the leakage reactance of transformer (pu), $V_i$isthe input voltage (pu), φ is the phase shift angle, andV_0 is the output voltage (pu).

B. Two-stage configuration

The two-stage comprises of DC-link in either MV side or LV side. The power flow can either be bidirectional or unidirectional depending on the usage. The stage offered better reactive power compensation than the single-stage, nevertheless, the design and switching process is more complex than the single-stage configuration. The stage cannot operate at a high voltage level and is also not suitable for renewable energy integration when the DC-link is at the low voltage side.

C. Three-Stage configuration.

Three-stage is the most common configuration. The stage comprises DC–links on the MV side and the LV side. The stage is suitable for use in both transmission and distribution systems and offers better performance with respect to fault isolation and power quality regulation Also, the configuration is more scalable than other configurations, however, it has high conduction and switching losses due to the many conversion stages involved and thus reduces the efficiency. The reduction in weight and volume of the transformer makes its application to be diverse; PET is suitable for onboard electric traction, battery charger, off-shore wind farm, and tidal power. It is also suitable for use for microgrid integration.

The schematic diagrams of all three configurations are shown in Fig 1.

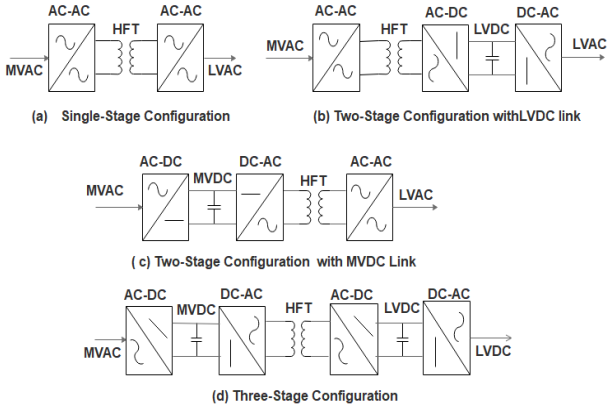

Fig 1. Power Electronic Transformer Configuration

III. METHODOLOGY

The PET device is modelled using the equations below. The parameters used in the simulation are calculated using the Eq.2 – Eq.4 and Eq.11 – Eq.16. The parameters are: (1) grid line to line voltage 11kV, (2) line filter inductance 624 mH (3) line filter capacitance 20µF, (4) line filter damping resistance 5Ω, (5) DC-link medium voltage side capacitor (Cdc1= Cdc2) 1500000 mF, (6) HFT operating frequency 2 kHz, (7) Arm resistance 0.5Ω (8) arm inductance 550mH, (9) DC-link low voltage side capacitor (Cdc3 = Cdc4) 7500µF, (10) load filter inductance 1mH,(11) load filter capacitance 470µF, (12) load filter resistance 0.2Ω , (13) LV side line-line voltage 0.415 kV, (14) PET rated power 500 kVA.

The procedure used for the modelling the PET device is described below.

D. Steady State Modelling and Simulation

A 3-phase 11 / 0.415kV, 500 kVA three-stage topology is presented. The block diagram of the PET device with a load is depicted in Fig.2.

This PET device has three stages that is the input stage, isolation stage, and output stage. The input stage consists of 3-phase rectifier which converts the alternating MV to DC voltage while the isolation stage comprises of an inverter, HFT in the centre and rectifier. The inverter and a rectifier correspond to the MV (primary side) and LV (secondary side) of the HFT respectively. The MVside inverter converts the DC voltage into a high-frequency PWM voltage signal which is then applied to the primary side of the HFT. The secondary-side alternating PWM voltage signal is now transformed to a low voltage DC waveform by the LV-side rectifier. The output stage employs a 2-level 3-phase inverter which convert the low voltage DC to AC and, it is then connected to the LV (0.415kV) distribution feeder and loads.

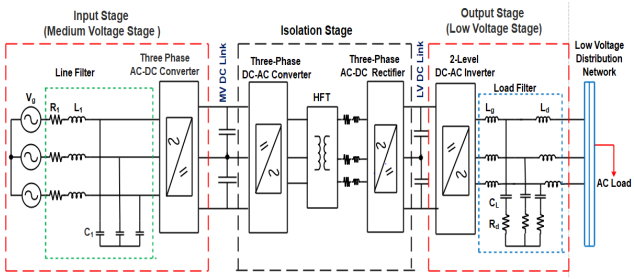

Fig 2. Three Stage Power Transformer Configuration.

E. Input stage of three stage PET

The input stage is made up of a three-level, three-phase IGBT bridge PWM converter connected to a three-phase medium voltage distribution network via a damped LC filter. The complete configuration of the input stage with damping filter and control scheme is shown in Fig 3.

The input current, keeping the DC-link voltage at the desired reference value and input power factor are determined by the rectifier control system, and it is developed in the rotating d-q reference [19], [20].

The input stage is mathematically model in d-q reference frame as given in Eq. 2 and Eq. 3.

$$L_{E1}\frac{\partial i_{E1d}}{\partial t} = \omega L_{E1} i_{E1q} + V_{1d} - V_{E1d} \quad (2)$$

$$L_{E1}\frac{\partial i_{E1q}}{\partial t} = \omega L_{E1} i_{E1d} + V_{1q} - V_{E1q} \quad (3)$$

where, $V_{E1} = [V_{E1a},\ V_{E1b,}V_{E1c}]$ is the AC terminal voltage vectors in the primary side, L_{E1} is the interface inductances, $V_1 = [V_{1a}, V_{1b}, V_{1c}]$ is input voltage in the primary, i_{E1} is the line current $[i_{Ea}, i_{E1b}, i_{E1c}\ ]$vectors in the primary sideand $\omega$is the synchronous angular of the grid voltage.

The output voltage of the 3-level PWM rectifier id controlled by i_{ds} and i_{qs}, and an assumed constant voltage. The system double closed-loop control design in d-q reference frame is based on Eq. 4 and Eq. 5.

$$V_d^* = -\left(K_{ip} + \frac{K_{i1}}{S}\right)(i_d^* - i_{sd}) + \omega L_{isq} + V_{sd} \quad (4)$$

$$V_q^* = -\left(K_{ip} + \frac{K_{i1}}{S}\right)(i_q^* - i_{sq}) - \omega L_{isd} + V_{sq} \quad (5)$$

where K_{ip} and K_{i1} are the control coefficient

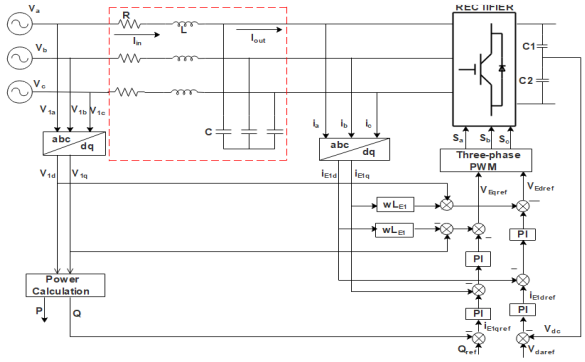

Fig 3 Input stage configuration and control scheme

The criterion for the dimensioning of the filter capacitors is to minimize the phase shift between the input current I_{in} and output current I_{out} of the filter [17], [18]. The capacitance of the capacitor is given as:

$$C_1 = \frac{\sqrt{3} I_{min} \tan Q_{max}}{\omega V_c} \qquad (6)$$

Where I_{min} is the transformer minimum permissible current, Q_{max} is the maximum possible phase shift between the input and output current, ω is the resonance frequency, and $V_c$is the capacitor voltage.

The inductance is given as:

$$L_1 = \frac{1}{f_c C_1} \qquad (7)$$

Where f_c is the cut-off frequency and C_1 is the filter capacitor.

The damping resistance is given as:

$$R_1 = \frac{Z_{in}}{2\zeta} \qquad (8)$$

$$Z_{in} = \sqrt{\frac{L_1}{C_1}} \qquad (9)$$

where ζ is the filter damping coefficient.

The reference voltage is compared with the rectifier output voltage and the error is combine with the proportional-integral (PI) controller to produce the reference value (i_d^*) while the reactive current reference i_q^* is set at zero.

The mathematical model and control of a 3-phase controlled rectifier are presented in [21].

F. Isolation stage and control

This stage consists of the HFT and the inverter and rectifier which are place on the input (primary side) and outer (secondary side) of the HFT respectively as shown in Fig 4. This stage also used for galvanized isolation between the input and output stage.

The HFT is responsible for the small size and weight of the PET device when compare to the conventional transformer. It allows the transformer to operate at a higher frequency and allows high voltage and current ratios between the input and output of the HFT. The output rectifier provides the required DC link voltage for the PET output stage and the active power flow depends on the phase shift ratio between the voltage on the primary and the secondary of the HFT.

The input and output loops are used to regulate the transformer inductance current i_{dc2} and capacitor voltage V_{dc2} respectively.

The input and output loops help to speed up control response and reject oscillations.

The transformer average power is given as:

$$P_{AV} = \frac{\left({}^{V_{dc1}}/_{M}\right) \cdot V_{dc2}}{\omega \cdot L} \cdot \varphi \cdot \left(1 - \frac{|\varphi|}{\pi}\right) \qquad (10)$$

where M is the HFT ratio, and ω is the angular frequency, $L$is the leakage inductance of secondary side transformer, V_{dc1} and V_{dc2} are the capacito voltages, and φ is the phase shift angle.

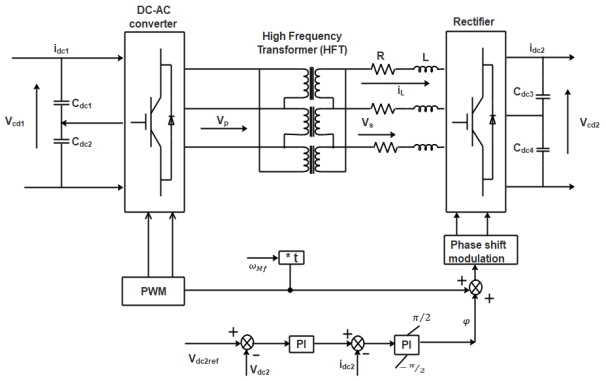

Fig. 4. Isolation Stage configuration

G. *Output stage configuration and control*

The output stage comprises of two-level three-phase inverter connected to a low voltage distribution network and load as shown via a dapping LCL filter as depicted in Fig 5. This stage provides constant amplitude and frequency of the voltage to the load. The transformer should be able to respond to changes in load within a certain range and maintain the amplitude of the output voltage during grid disturbances.

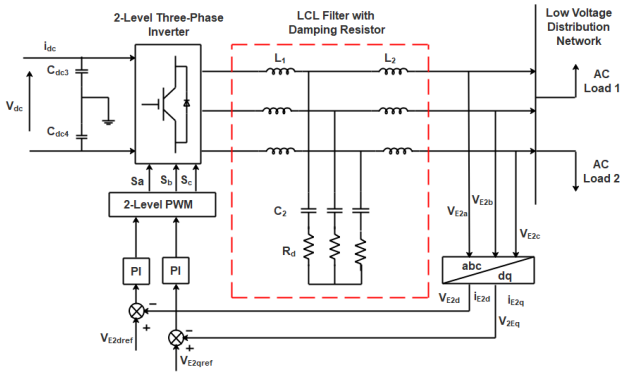

Fig 5. Output Stage Configuration

The LCL filter parameters can be calculated using the following equation [22]. The inverter side inductance (L_1) and the load side inductance (L_2) are given in Eq.11 and Eq.12:

$$L_1 = \frac{V_{dc}}{6f_{sw}\Delta I_{LMAX}} \quad (11)$$

$$L_2 = rL_1 \quad (12)$$

where ΔI_{LMAX} is the variation in ripple current, f_{sw} is the switching frequency and V_{dc} is the DC link voltage.

The change in the ripple current is given as:

$$\Delta I_{LMAX} = 0.1\left(\frac{P\sqrt{2}}{3V_{ph}}\right) \quad (13)$$

The capacitance of the capacitor is given as:

$$C_2 = 0.5C_b \quad (14)$$

Where $C_b = \frac{1}{f_g Z_b}$, $Z_b = \frac{V_{LL}^2}{P}$,

f_g is the grid frequency, , C_b is the base capacitance and P is the active power Z_b is the base impedance, and V_{LL} is the line-to-line voltage.

The resonance frequency and the damping resistance are given in Eq. 15 and Eq. 16.

$$f_{res} = \frac{1}{2\pi}\sqrt{\frac{L_1+L_2}{(L_1)(L_2)C_2}} \quad (15)$$

$$R_d = \frac{1}{3f_{res}C_2} \quad (16)$$

The output stage phase mathematical model is described in Eq.17 and Eq.18.

$$L_{E2}\frac{\partial i_{E2d}}{\partial t} = \omega L_{E2} i_{e2q} + V_{2d} - V_{E2d} \quad (17)$$

$$L_{E2}\frac{\partial i_{E2q}}{\partial t} = -\omega L_{E2} i_{E2d} + V_{2d} - V_{E2q} \quad (18)$$

IV. RESULTS AND DISCUSSION

Fig. 6 (a) shows a perfect source voltage and current from the MV side of the grid while Fig 6 (b) shows the HFT primary and secondary voltage of the PET device. As can be seen in Fig 6, the 3-level rectifier convert the grid voltage with a unity power factor into a high voltage DC of 18 kV as depicted in Fig 7. the 3-level converter modulates the DC voltage to a high-frequency square wave and the step-down to a DC voltage of 600 V by HFT as depicted in Fig 8. This conversion corresponds with characteristic of the 0.415kV AC distribution network

To investigate the behaviors of the PET device, different loads were applied to the transformer so as

to evaluate its performance. when a 310kVA was connected to the transformer, the system provides a perfect voltage and current waveform, and they were within the design specification of the LV network as depicted in Fig 9. Also, when a pure resistive load of 300 kW was connected, it gave a perfect waveform with a reduction in current as expected, as depicted in Fig 10. It was observed that with pure resistive load, the voltage and current reduce in amplitude.

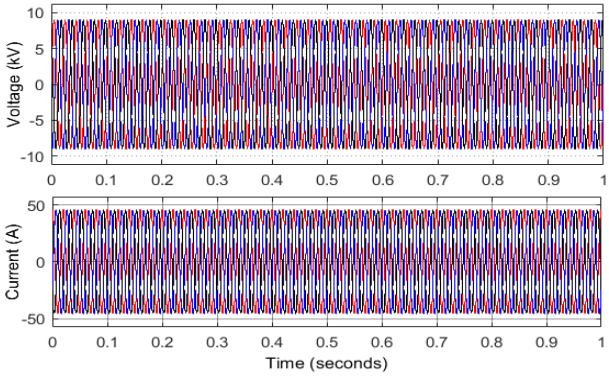

(a) Source voltage and current

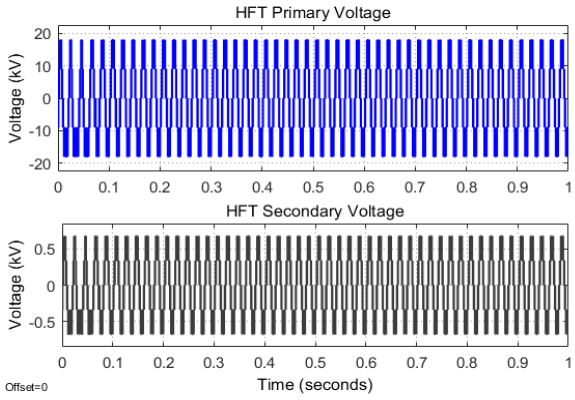

(b) HFT Primary and secondary voltages

Fig. 6 shows the steady-state characteristic waveforms, including (a) source voltage and current, (b) HFT primary and secondary voltage

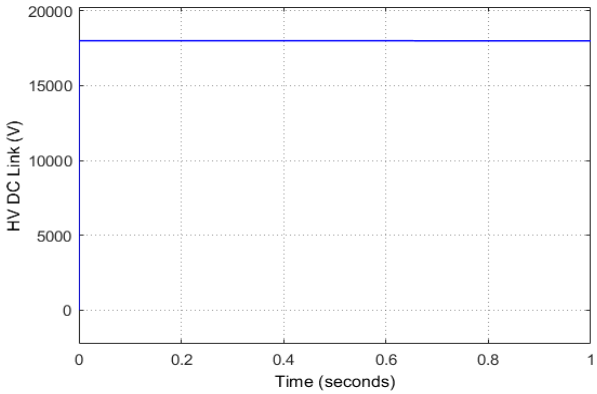

Fig 7. High DC-link Voltage of 18000V

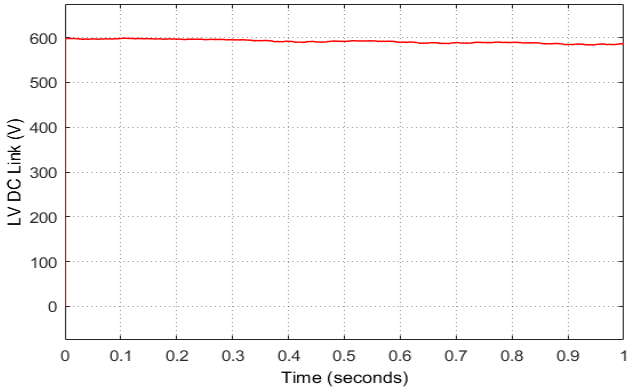

Fig 8.Low DC-link Voltage of 600 V

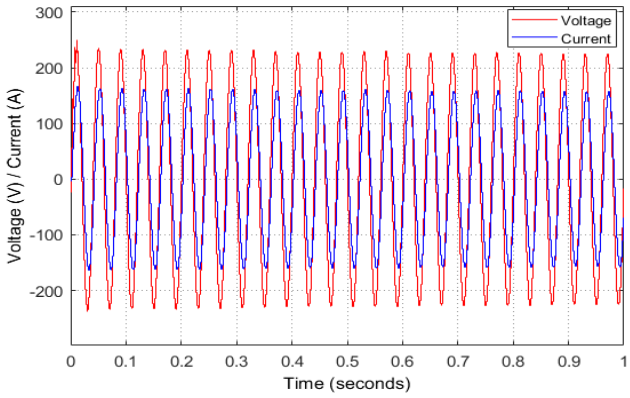

Fig.9 (a) Load voltage and current at 310kVA

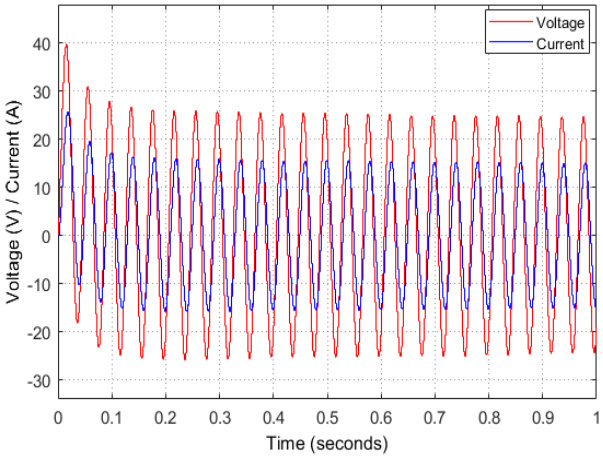

Fig.10. Voltage and current at 300kW pure resistive load

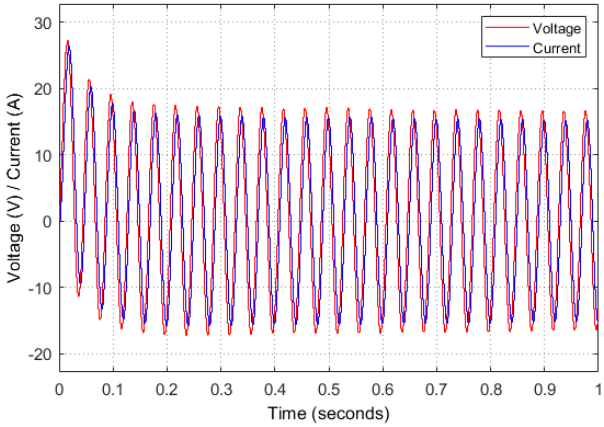

Fig 12. Voltage and current at 50% increase in a purely resistive load

As can be seen in Fig. 11, it was observed that a 50 % increase in load, causes the load current to increase while the voltage maintains constant amplitude.Contrary, a 50 % increase in pure resistive load causes a reduction in voltage while the current maintains a constant amplitudeas seen in Fig 12. On the other hand, 50 % reduction in load causes a reduction in the current while the voltage maintains a constant amplitude as seen Fig.13. Also, a 50% reduction in pure resistive load maintains a constant current amplitude with an increase in voltage amplitude as shown in Fig. 14. The results show the efficacy of the PET device.

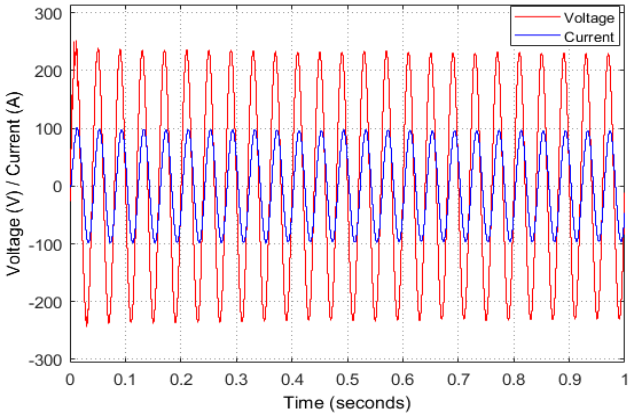

Fig.13. Load voltage and current at 50% reduction in load

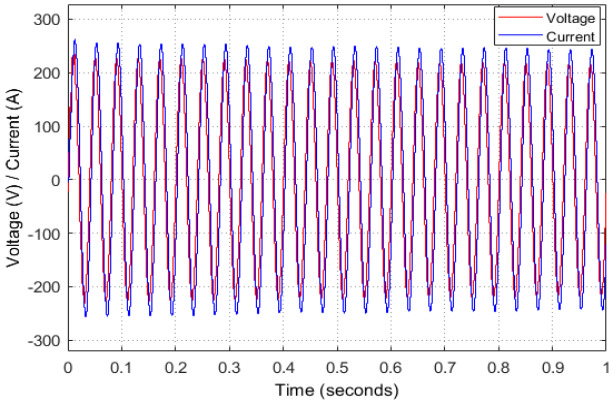

Fig.11 Load voltage and current at 50% increase in load

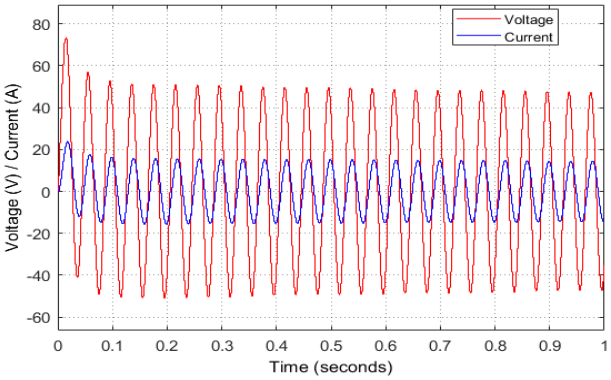

Fig.14. (f) voltage and current at 50% reduction in pure resistive

V. CONCLUSIONS

This paper designed and simulate a 500 kVA PET device for use on an LV distribution network. The parameters of the PET device and filters were calculated and simulated, and, the simulation results shows that DC link voltage, input and output voltage are within the design specification for 11 / 0.415 kV.

The designed PET device produces quality voltage and current waveform, and performs very well under different condition which shows that the transformer is capable of adjusting itself to different load conditions, and can replace the traditional LV transformers in the nearest future.

REFERENCE

[1] C. Ling, B. Ge, D. Bi, and Q. Ma, "An effective power electronic transformer applied to distribution system," 2011 Int. Conf. Electr. Mach. Syst. ICEMS 2011, 2011.

[2] J. Wang et al., "Power electronic transformer with adaptive PLL technique for voltage-disturbance ride through," J. Mod. Power Syst. Clean Energy, vol. 6, no. 5, pp. 1090–1102, 2018.

[3] L. Heinemann and G. Mauthe, "The universal power electronics based distribution transformer, an unified approach," PESC Rec. - IEEE Annu. Power Electron. Spec. Conf., vol. 2, pp. 504–509, 2001.

[4] G. Quartarone, M. Liserre, F. Fuchs, N. Anglani, and G. Buticchi, "Impact of the modularity on the efficiency of Smart Transformer solutions," IECON Proc. (Industrial Electron. Conf., pp. 1512–1518, 2014.

[5] J. S. Lai, A. Maitra, A. Mansoor, and F. Goodman, "Multilevel intelligent universal transformer for medium voltage applications," Conf. Rec. - IAS Annu. Meet. (IEEE Ind. Appl. Soc., vol. 3, pp. 1893–1899, 2005.

[6] M. A. Hannan et al., "State of the art of solid-state transformers: Advanced topologies, implementation issues, recent progress and improvements," IEEE Access, vol. 8, pp. 19113–19132, 2020.

[7] Z. Qu, Y. Yao, Y. Wang, C. Zhang, Z. Chong, and A. Abu-Siada, "A novel unbalance compensation method for distribution solid-state transformer based on reduced order generalized integrator," IEEE Access, vol. 7, no. Mmc, pp. 108593–108603, 2019.

[8] I. Syed and V. Khadkikar, "Replacing the Grid Interface Transformer in Wind Energy Conversion System with Solid-State Transformer," IEEE Trans. Power Syst., vol. 32, no. 3, pp. 2152–2160, 2017.

[9] X. She, A. Q. Huang, and R. Burgos, "Review of solid-state transformer technologies and their application in power distribution systems," IEEE J. Emerg. Sel. Top. Power Electron., vol. 1, no. 3, pp. 186–198, 2013.

[10] J. W. Van Der Merwe and H. Du, "The solid-state transformer concept: A new era in power distribution," IEEE AFRICON Conf., 2009.

[11] D. Wang, C. Mao, and J. Lu, "Operation and control mode of electronic power transformer," 1st IEEE-PES/IAS Conf. Sustain. Altern. Energy, SAE 2009 - Proc., 2009.

[12] G. De Carne, G. Buticchi, M. Liserre, and C. Vournas, "Load Control Using Sensitivity Identification by Means of Smart Transformer," IEEE Trans. Smart Grid, vol. 9, no. 4, pp. 2606–2615, 2018.

[13] G. De Carne, G. Buticchi, Z. Zou, and M. Liserre, "Reverse Power Flow Control in a ST-Fed Distribution Grid," IEEE Trans. Smart Grid, vol. 9, no. 4, pp. 3811–3819, 2018.

[14] N. Kimura, T. Morizane, I. Iyoda, K. Nakao, and T. Yokoyama, "Solid state transformer investigation for HVDC transmission from offshore windfarm," 2017 6th Int. Conf. Renew. Energy Res. Appl. ICRERA 2017, vol. 2017-Janua, pp. 574–579, 2017.

[15] H. Qin and J. W. Kimball, "Ac-Ac dual active bridge converter for solid state transformer," 2009 IEEE Energy Convers. Congr. Expo. ECCE 2009, no. c, pp. 3039–3044, 2009.

[16] R. T. Naayagi, A. J. Forsyth, and R. Shuttleworth, "High-power bidirectional DC-DC converter for aerospace applications," IEEE Trans. Power Electron., vol. 27, no. 11, pp. 4366–4379, 2012.

[17] S. Pinto and J. Silva, "Input Filter Design of a Mains Connected Matrix Converter," no. October 2006, pp. 1–7, 2006.

[18] D. R. Pereira, S. F. Pinto, and J. F. Silva, "Power Electronic Transformer as a Solution for Voltage and Frequency Regulation in Isolated Electrical Networks," pp. 1–9.

[19] K. Y. Ahmed, N. Z. Yahaya, V. S. Asirvadam, and O. Ibrahim, "Modeling and Simulation of Power Electronic Distribution Transformer Based on a Three Level Converter," Appl. Mech. Mater., vol. 785, pp. 151–155, 2015.

[20] K. Y. Ahmed, N. Z. Yahaya, and V. S. Asirvadam, "Optimal analysis and design of power electronic distribution transformer," Res. J. Appl. Sci. Eng. Technol., vol. 7, no. 9, pp. 1734–1743, 2014.

[21] V. Blasko and V. Kaura, "A new mathematical model and control of a three-phase AC-DC voltage source converter," IEEE Trans. Power Electron., vol. 12, no. 1, pp. 116–123, 1997.

[22] A. E. W. H. Kahlane, L. Hassaine, and M. Kherchi, "LCL filter design for photovoltaic grid connected systems," Third Int. Semin. new Renew. energies, vol. 8, no. 2, pp. 227–232, 2014.

